Nuclear Instruments and Methods in Physics Research A 735 (2014) 431–436

Contents lists available at ScienceDirect

Nuclear Instruments and Methods in Physics Research A

journal homepage: www.elsevier.com/locate/nima

# MCNP benchmarking of an inelastic neutron scattering system for soil carbon analysis

Oded Doron [a,*,1], Lucian Wielopolski [b], Sudeep Mitra [c], Steven Biegalski [d]

[a] Sandia National Laboratory, 1515 Eubank, Bldg. 758, MS 0406, Albuquerque, NM 87123, USA
[b] Brookhaven National Laboratory, Environmental Sciences Department, Bldg. 490, Upton, NY 11973, USA
[c] Brookhaven National Laboratory, Environmental Sciences Department, Bldg. 490, Upton, NY 11973, USA
[d] The University of Texas at Austin, 1 University Station, Austin, TX 78759, USA

ARTICLE INFO

*Article history:*
Received 18 June 2012
Received in revised form
21 September 2013
Accepted 21 September 2013
Available online 8 October 2013

*Keywords:*
Monte Carlo
Soil analysis
Carbon
Benchmarking
Gamma-ray neutron transport

ABSTRACT

We benchmark here a Monte Carlo model simulating an inelastic neutron scattering (INS) system for quantitative analysis of carbon in soil. Specifically, we compare the simulations with experimental results of copper foils activations, INS system calibration, INS system optimization of the height above the ground and comparing pulse height distributions due to $^{137}$Cs and $^{60}$Co sources. Most of the simulations and the measurements agree better than 10%, although some of them registered discrepancies larger than 20%.



## 1. Introduction

The centrality of soil carbon: in global carbon cycle, in soil quality management practices, in land restoration, in monitoring terrestrial sequestration, and in precision agriculture are only but a few examples implicating soil carbon in extensive research worldwide. The need for assessing carbon inventories in soil on large spatial and temporal scales with reduced uncertainties stimulated novel implementations of three independent, well-established analytical techniques for soil analysis. These are near-infrared spectroscopy (NIR) [1,2], laser-induced breakdown spectroscopy (LIBS) [3], and inelastic neutron scattering (INS) [4]. These three techniques respectively entail spectroscopy on the molecular-, atomic-, and nuclear-levels. The INS method can be simulated using Monte Carlo (MC) codes for gamma-neutron transport calculations. These codes enable complex system simulations which otherwise would be time consuming, costly, and occasionally impossible to perform. These simulations can be performed with an arbitrary degree of detail provided that all the basic data and complete system description are available. One of these codes that has been widely used for radiation transport in soil is the Monte Carlo N-Particle (MCNP) transport code, developed at Los Alamos National Laboratory [5,6]. For example, MCNP has been used for evaluating soil activation, radiation shielding in soil, in the well logging industry, and for design of complex gauges based on nuclear techniques. One such technique, which gained widespread use, is in situ, non-destructive, multi-elemental analysis of bulk geological samples using neutrons [7,8]. In this work we benchmark a MC model of the INS technique by comparing MCNP simulations with experimental results using: (1) Cu foil activations, (2) INS system calibration, (3) INS system positioning above the ground and (4) measured gamma-ray pulse height distribution.

## 2. Methods

### 2.1. INS system

Inelastic neutron scattering is a fairly new method for in field soil carbon analysis that is non-destructive, multi-elemental, and uniquely probes large volumes, greater than 0.3 m$^3$. The method can be used in static and scanning modes of operation [9]. The method is based on nuclear reactions of fast, 14 MeV, neutrons undergoing INS and thermal neutron capture interactions with carbon and other soil elements' nuclei. These processes stimulate emissions of 2.22 (thermal neutron capture), 4.43 (INS), and 6.13 (INS) MeV gamma-rays in hydrogen, carbon and oxygen, respectively.

* Corresponding author. Tel.: +1 505 284 6875, fax: +1 505 284 6135.
*E-mail addresses:* odeddo@yahoo.com (O. Doron), lwielo@bnl.gov (L. Wielopolski), smitra@bnl.gov (S. Mitra), biegalski@mail.utexas.edu (S. Biegalski).
[1] Present address: Sandia National Laboratory, 1515 Eubank, Bldg. 758, MS 0406, Albuquerque, NM 87123, USA.

0168-9002/$ - see front matter © 2013 Elsevier B.V. All rights reserved.
http://dx.doi.org/10.1016/j.nima.2013.09.049

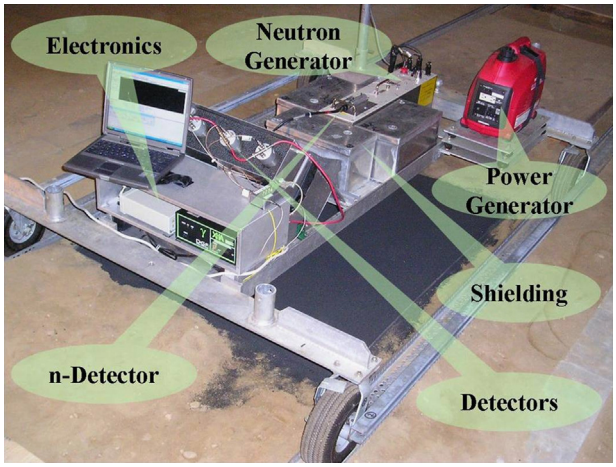


**Fig. 1.** An alpha prototype of the INS system.

The fast neutrons are produced by a (d,t) neutron generator (NG) and the induced gamma-rays are detected by an array of three NaI detectors separated by shielding from the NG. The entire system is placed on a cart about 30 cm above the ground. An alpha prototype of an INS system in Fig. 1 shows the main components of the system that were simulated in subsequent studies. Several field studies demonstrated the utility of the system [4,10].

### 2.2. MCNP model

Two major components constitute complete INS simulation; (1) the INS system with its components and geometry and (2) the soil in which fast neutrons induce the gamma-rays that interact with the detection system. The complexity of the soil three phase components that may change in their composition and distributions are well established [9]. The measured carbon signal depends on the transport conditions of neutrons and gamma rays in the soil matrix, which are affected by the soil moisture and bulk density. While variations in the bulk density affect both the neutron and the gamma ray attenuation, the moisture affects mainly, but not only, the transport of neutrons due to elastic scattering with hydrogen nuclei. Changes in the transport properties of the soil influence the sampling depths thus affecting the calibration and response function of the INS system.

The response function, $R$ in Eq. (1), for the INS system accounts for the transport of gamma-rays and neutrons in soil and cannot be solved analytically and its complexity makes any numerical solution very cumbersome and highly inefficient.

$$\int_{E_{thr}}^{E_{max}} \phi_n(x,y,z,E_n)\sigma(E)C_c(x,y,z)\rho_b(x,y,z)\Omega(x,y,z)At(x,y,z)dEdxdydz$$

$$R \propto \int_0^T dt \int_{-\infty}^{\infty}\int_{-\infty}^{\infty}\int_h^{\infty}\int\int_{V'}\int Det(E_\gamma,x',y',z')dx'dy'dz' \qquad (1)$$

where $T$ is the time domain, $E$ is the neutron energy from incident energy of 14 MeV down to carbon inelastic scatter threshold energies 4.43 MeV, $V$ is the soil space, which is semi-infinite in all directions, and $V'$ is the space occupied by the detectors. The simulation is limited to a parallelepiped volume of 250 cm by 200 cm and 50 cm deep. Inherent lateral homogeneity is assumed in this model. Thus, the number of counts in the carbon peak, which is proportional to $R$, depends on the depth distributions of the various components in the equation;

- $\varphi_n(x,y,z,E_n)$ (n/cm$^2$) is the calculated neutron-flux depth distribution that decreases with depth.
- $\sigma(E)$ (cm$^2$) is the inelastic neutron scatter cross-section that is only dependent on the neutron energy.
- $C_c(x,y,z)$ (gC/cm$^3$), the carbon-depth profile usually decreases with depth, although it may assume different distributions.
- $\rho_b(x,y,z)$ (g/cm$^3$), the soil's bulk density increases with depth.
- $\Omega(x,y,z)$ (fraction), the solid angle subtended by the detectors from the emission point of the gamma-rays in the soil.
- $At(E_\gamma,x,y,z)$ (fraction), the attenuation of gamma-rays on their way to the detector, increases with depth.
- $Det(E_\gamma,x',y',z')$ (photopeak counts) is the detector response function. It is used to calculate the energy deposition in a detector and allocation in a spectrum.

The MC method enables very accurate modeling of arbitrarily complex systems thus replacing complicated experiments or enabling numeric simulation of ones that cannot be performed at all. There are several well established MC codes in use, for example PHOTON and EGS [11,12]; the one used in the present work is MCNP Version 5 [5,6]. This is a very robust extensively used code for particle transport in soil, for example it was used to model the measurement of chlorine with prompt gamma-ray neutron activation analysis, for assessing the sensitivity of neutron- and gamma-fluxes in soils saturated with fresh water, salty water, oil and others [13].

In this work we present several experiments and simulations that were performed to benchmark a MCNP5 model of the INS system. The benchmarks concentrate on different parts of the model. The benchmarking is considered satisfactory when an agreement between experiments and simulations is achieved within 10% [14].

### 2.3. Cu foil activation

A neutron flux foil experiment was performed to benchmark the MCNP5 modeling of the neutron transport of the system; comparing the measured neutron generator flux at several stand-off locations to simulations. Fast, 14 MeV, neutron generators outputs are frequently monitored using the Texas Convention Technique [15,16]. Accordingly, Cu foils with known weights are irradiated at known location from the neutron generator focal point and the induced activity at 511 keV is counted using NaI detectors. The reaction involved is that of $^{63}$Cu (n,2n) $^{62}$Cu in which the daughter decays by positron emission with a half-life of 9.9 min. The cross-section for this reaction is ~500 mili-barns and with a threshold energy of 11.3 MeV provides a good measure of the un-collided fast neutron flux.

The radiation induced activity $\lambda N$ in a Cu foil is given in Eq. (2),

$$\lambda N = \sigma\varphi N_T(1-e^{-\lambda T_i}) \qquad (2)$$

in which: $\lambda$ is the decay time constant of $^{62}$Cu (1/s), $N$ is the number of radioactive atoms, $\sigma$ is the cross-section for the (n,2n) reaction, $\varphi$ is the neutron flux at the location of the foil, $N_T$ is the total number of $^{63}$Cu atoms (natural abundance is 69.17%) in the target and $T_i$ is the irradiation time. The number of counts $C$ in a counter resulting from Cu foil activity is given in Eq. (3),

$$C = k\sigma\varphi N_T(1-e^{-\lambda T_i})e^{-\lambda T_d}(1-e^{-\lambda T_c}) = K\varphi \qquad (3)$$

where $k$ is a proportionality constant, involving for example; total counter efficiency, Cu foil decay modes etc. and $K$ combines all the constant terms; $T_d$ is the time between the end of the irradiation and the beginning of the counting and $T_c$ is the counting time.

Thus, based on the fast neutron flux, $\varphi$, at the Cu foil in Eq. (3), we can derive the fast neutron flux at the source, i.e., the focal point in the neutron generator, $\varphi_0$, as the flux at the Cu foil is

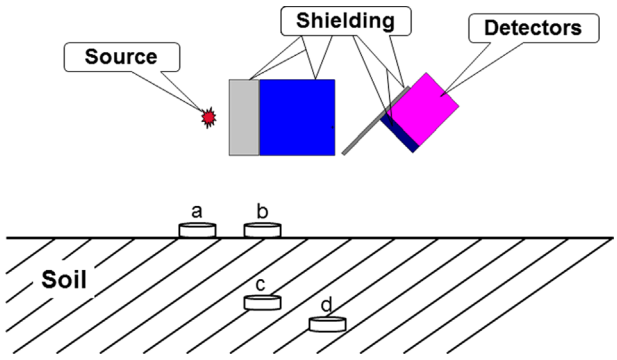


**Fig. 2.** The approximate placement of the four copper flux foils, not to scale.

corrected by the distance r from the foil,

$$\varphi_0 = (C/K)4\pi r^2 \quad (4)$$

Following an irradiation time of 3600 s, a decay time of 30 s; while foils were transferred to a well-type NaI detector, the foils were counted for 600 s. The copper foils were 99.9% pure, 0.1 cm thick, 2 cm in diameter and each weighted 3.29 g. The experimentally determined fluxes were compared to volumetric neutron path length tallies, e.g. flux, F4, by MCNP5.

Four experiments were performed with the copper foils placed at various locations; (1) on top of the soil 34 cm along the NG target line (line from the NG target perpendicular to the soil), (2) on top of the soil 7.5 cm away from the target line, (3) 13 cm below the soil top and 7.5 cm away from the target line, and (4) 18 cm below the soil top and 13 cm away from the target line. These locations are marked in Fig. 2 as position a, b, c, and d, respectively.

### 2.4. INS system calibration

Calibration of the INS systems was carried out using a 1500 kg batch of clean silica and a batch of silica homogeneously mixed with 10% by weight (150 kg) carbon. The latter was subsequently diluted by a factor of two twice. These synthetic soils were placed in a wooden box that rested on the ground with dimensions 1.52e6 × 1.22e6 × 4.6e6 $cm^3$ and measured four times at each concentration; the soil bulk density was determined to be about 1400 kg $m^{-3}$ (1.4 g $cm^{-3}$). The MCNP5 calculated number of carbon 4.43 MeV gamma-rays intercepting the detectors, calculated using an F4:p tally with energy windows, was compared with the measured carbon peak intensities. Based on observations and calculations, and due to the volume and size of the box, we believe that the surrounding materials did not contribute anything measurable.

### 2.5. INS response versus height

The NG and the detectors are mounted on a cart, the height of which is optimized to maximize the counting yield. Increasing the height reduces the signal due to increase in the inverse distance squared. On the other hand, increase in the height increases the footprint from which the signal is collected. MCNP5 simulated gamma-ray yields for silicon at 1.78 MeV, carbon at 4.43 and oxygen at 6.13 MeV were compared with experimentally determined net peak areas in measured spectra. To accommodate the increased height the simulated volume was increased to 800 cm by 800 cm by 60 cm deep. Key soil parameters: composition, moisture and density remained the same throughout all the calculations with the exception of the dimensions of the soil volume which was increased to 800 cm by 800 cm by 60 cm deep.

### 2.6. Detector's pulse height distribution

The benchmarking of the detector pulse height distribution with MCNP5 is a more complicated matter than the benchmarking of the gamma and neutron transport. The pulse height of a detector is affected by many factors, including but not limited to, crystal size, efficiency, and electronics, which all have to be taken into account in the model. The final benchmarking of the MCNP5 code was performed by comparing a simulated pulse height distribution from a detector, using pulse height (F8) tallies with measured gamma-ray spectra. The measured spectra included a background spectrum and two spectra using $^{137}Cs$ and $^{60}Co$ calibration sources.

## 3. Results

### 3.1. Cu foil activation

The activities of the Cu foils counted in a well-type NaI(Tl) scintillation detector were converted using Eq. (3) to neutron fluxes (n $cm^{-2}$ $s^{-1}$) and, subsequently, using Eq. (4) to NG outputs (n $s^{-1}$). The NG output determined from the experimental flux at position "a" was taken as the reference output of the NG and all subsequent simulations are multiplied by the NG output to convert the flux in n $cm^{-2}$ (source particle)$^{-1}$ to n $cm^{-2}$ $s^{-1}$. The key parameters for the n,2n reactions and timing conditions used in these experiments are summarized in Table 1. The last three rows in Table 1 are the results for a Cu foil activation in position a. These include the net number of counts in an activated foil; the n-flux at the foil position, using Eq. (3); and the NG output, calculated using Eq. (4). The experimental results and MCNP5 calculations of the neutron fluxes at the positions of the Cu foils are summarized in Table 2. The discrepancies of up to 10% between experimentally determined and calculated neutron fluxes may be attributable to the errors in positioning of the Cu foil, modeling of the soil, and shielding materials.

### 3.2. INS system calibration

System calibration was benchmarked by comparing the carbon mean gamma-ray flux intercepting the detection volume with the carbon peak net area in the measured spectra. These results are summarized in Table 3 in which column 2 contains the calculated gamma-ray flux for the carbon region of interest (ROI) centered around 4.43 MeV intercepting the detection volume. In column 3, the net gamma-ray flux, is given by subtracting the background flux due to zero concentration of carbon. In column 4 the net results are normalized to the experimental value with the highest carbon concentration of 0.14 gC $cm^{-3}$, i.e., all net results are

**Table 1**
Basic parameters of the Cu foil and experimental counting setup for Cu foil in position 'a'.

| Gamma ray energy of $^{63}Cu(n,2n)^{62}Cu$ (keV) | 511 |
|---|---|
| Half-live (s) | 594 |
| Cu foil mass(g) | 3.29 |
| Cu number of atoms | 3.12 $10^{22}$ |
| n,2n cross-section (barns) | 0.48 |
| 511 keV gammas/disintegration | 0.972 |
| Counting efficiency at 511 keV | 0.11 |
| Source target distance (cm) | 33.97 |
| Irradiation time (s) | 3600 |
| Transfer time (s) | 30 |
| Counting time (s) | 600 |
| Cu foil counts | 712 ( ± 103) |
| n-Flux at foil (n $cm^{-2}$ $s^{-1}$) | 1084.2 |
| NG output (n $s^{-1}$) | 1.57 $10^7$ |

**Table 2**
Comparison of the neutron fluxes measured by Cu foils and calculated by MCNP5 at the foil level.The calculated neutron fluxes are above reaction threshold energy of 11.3 MeV. Note: MCNP5 errors less than 1%.

| n-Flux at the foil level ($n\,cm^{-2}\,s^{-1}$) | | | |
|---|---|---|---|
| **Position** | **Cu Foil** | **MCNP5** | **Diff(%)** |
| a | $1084 \pm 152$ | 1151 | 5.82 |
| b | $1020 \pm 122$ | 1078 | 5.39 |
| c | $376 \pm 130$ | 387 | 2.81 |
| d | $294 \pm 87$ | 269 | 9.26 |

**Table 3**
Results from the calibration experiment performed.

| Carbon concentration ($gC\,cm^{-3}$) | Gamma-ray flux per source neutron | | | Experimental |
|---|---|---|---|---|
| | Total 4.43 MeV gammas | Net 4.43 MeV gammas | Normalized net C counts | Net carbon counts |
| 0.0000 | $5.60 \times 10^{-8}$ | $0.00 \times 10^{0}$ | 0 | 0 |
| 0.0375 | $8.03 \times 10^{-8}$ | $2.43 \times 10^{-8}$ | 2466 | 1976 |
| 0.0500 | $9.08 \times 10^{-8}$ | $3.48 \times 10^{-8}$ | 3530 | – |
| 0.0700 | $1.03 \times 10-7$ | $4.75 \times 10^{-8}$ | 4813 | 4252 |
| 0.1400 | $1.49 \times 10-7$ | $9.28 \times 10^{-8}$ | 9408 | 9408 |

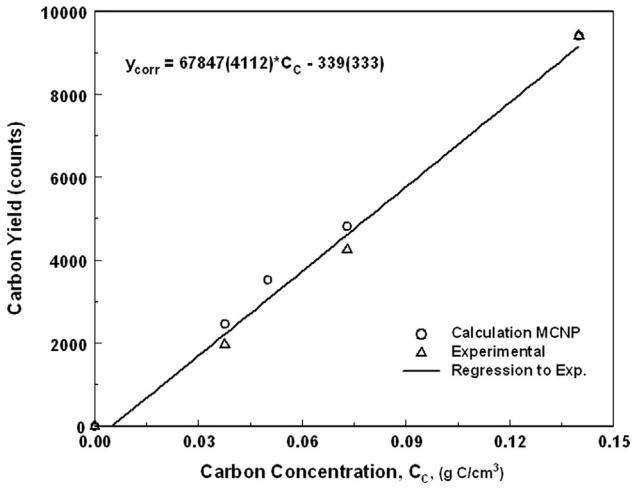


**Fig. 3.** Normalized MCNP5 calculations of the carbon yield overlaid with experimental results and regression line to the experimental results. $Y_{corr}$ in the linear regression fit indicates the carbon yield.

multiplied by $1.014 \times 10^{11}$ $(9408/9.28 \times 10^{-8})$. The results in Table 3 are plotted in Fig. 3. A line was fit to the experimental results with a linear regression fit. The MCNP5 calculations are systematically higher than experimental data when normalized at the highest point. The increasing discrepancy, up to 25%, suggests that either in the calculations or in experiments interference with the carbon peak is being overlooked. However, previously considerable work was done in measuring and correcting for interferences in the carbon peak [10]. These corrections were applied to the measurements presented here, therefore implying that either more work needs to be done to further understand the interferences in the carbon peak, or that higher fidelity modeling is necessary in follow on work.

### 3.3. Height optimization

The counting yields in the silicon, carbon, and oxygen peaks depending on the height of the system above the ground were

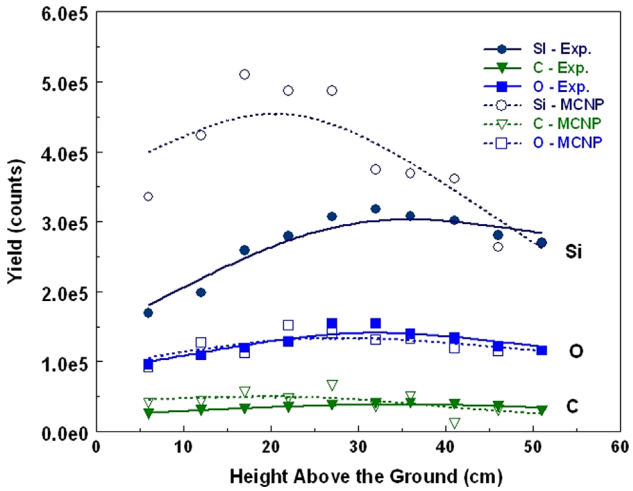


**Fig. 4.** MCNP5 predicted net number of counts in the peaks of carbon silicon and oxygen as a function of a distance of the INS system above the ground.

**Table 4**
Polynomials fitted to the height curves and the derived maxima.

| Coefficient | $X^2$ | $X$ | Constant | $X_{max}$ (cm) |
|---|---|---|---|---|
| Si–Exp | −180.8 | 12,606 | 91,542 | 35 |
| Si-MCNP5 | −4e-9 | 2e-7 | 4e-6 | 25 |
| O–Exp | −3.7 | 5276 | 61,248 | 31 |
| O-MCNP5 | −4e-9 | 2e-7 | 4e-6 | 25 |
| C–Exp | −22.3 | 1449 | 15,924 | 32 |
| C-MCNP5 | 1e-9 | 6e-8 | 2e-6 | 30 |

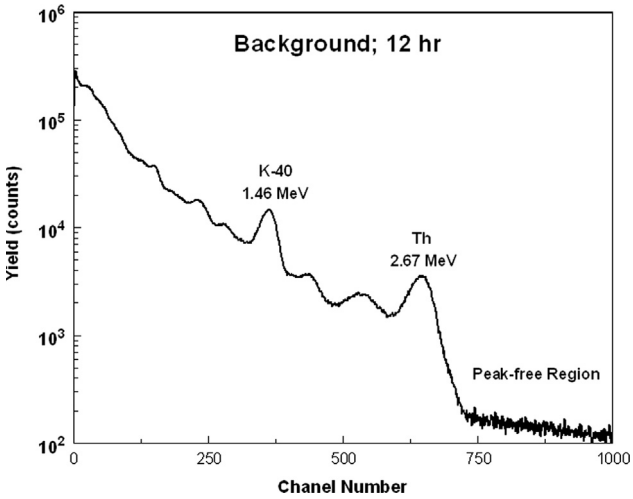


**Fig. 5.** Background spectrum counted for 12 h. Labeled on the plot are the K-40 and Th lines and peak-free region used for normalization.

simulated using MCNP5 and checked with field experiments. Since the exact elemental composition and distributions in the field are unknown the results cannot be compared directly. For example in MCNP5 simulations, oxygen has the most counts, whereas in the field experiment silicon has the most counts. MCNP5 simulations were normalized to field experiments by the ratio of the experimental to simulation's net peak areas at the maximum response height of each element. The maximum response height was calculated by fitting a second degree polynomial to the net peak areas from silicon, oxygen, and carbon, setting the derivative of each polynomial equal to zero and solving for $x$. The polynomial fits are shown in Fig. 4. The optimal heights derived from the fitted

**Table 5**
The net peak areas and the standard deviation (SD) of the $^{137}$Cs and $^{60}$Co peaks from experimental and MCNP5 simulated spectra. MCNP5 errors are from the statistical uncertainties of the resuls.

| | Detector 1 area (counts) | | Detector 2 area (counts) | | Detector 3 area (counts) | | Sum area (counts) | |
|---|---|---|---|---|---|---|---|---|
| **Peak** | **Exp** | **MCNP5** | **Exp** | **MCNP5** | **Exp** | **MCNP5** | **Exp** | **MCNP5** |
| $^{137}$Cs (662 keV)( ± SD) | 92,043(389) | 100,141(402) | 266,668(615) | 338,028(673) | 111,667(427) | 110,662(423) | 497,654(882) | 577,480(930) |
| $^{60}$Co (1173 keV) ( ± SD) | 9387(154) | 10,417(162) | 25,738(231) | 33,344(254) | 10,855(173) | 11,578(169) | 46,164(332) | 52,157(364) |
| $^{60}$Co (1332 keV) ( ± SD) | 9288(134) | 9526(139) | 24,656(209) | 30,512(219) | 11,207(153) | 10,568(145) | 48,283(311) | 43,664(320) |

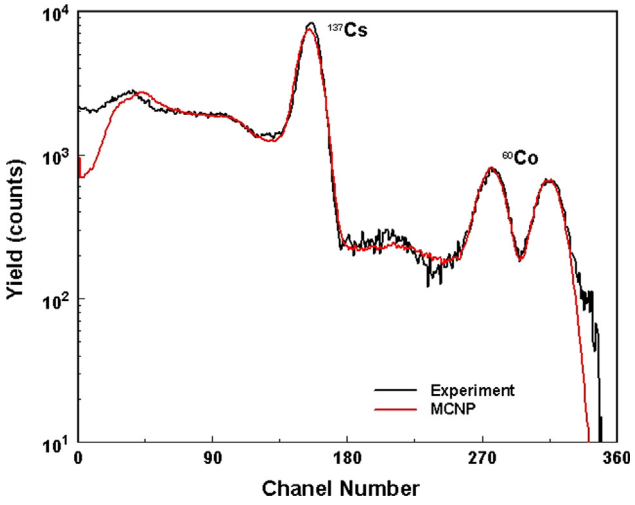


**Fig. 6.** Overlay of a simulated and a measured $^{137}$Cs/$^{60}$Co spectrum.

second degree polynomials together with the polynomials' coefficients are summarized in Table 4. The results agree within 5 cm. The lack of overlap of MCNP5 results with the experiments for Si peak is being investigated.

### 3.4. Cs and Co pulse height distributions

To simulate pulse height distributions (PHD) two calibrated point sources; a 26300 Bq $^{137}$Cs (661 keV) and 3220 Bq, $^{60}$Co (1173, 1332 keV), were used. The sources were placed 4 cm under each detector, one detector at a time. To simulate 10 min of counting time required $1.58 \times 10^7$ and $1.93 \times 10^6$ source particles for Cs and Co, respectively. The simulations were carried out using 0.85 branching ratio (gamma-rays per disintegration) for Cs source and Co/Cs intensity ratio of 0.144. Combined $^{137}$Cs/$^{60}$Co spectra and background spectra were acquired separately. The energy broadening of the peaks, required when simulating PHDs were determined from the full width half maxima (FWHM) of the measured peaks [17]; these are required as input parameters for a built in Gaussian energy broadening function in the MCNP5 code. The FWHM as a function of the square root of the energy is expressed as $0.1947\sqrt{E}-0.1014$. The $^{137}$Cs/$^{60}$Co sources and the detectors' FWHM were modeled in MCNP5.

The $^{137}$Cs/$^{60}$Co spectra were collected for 10 min while the background was collected for 12 h, Fig. 5. Due to the difficulty to simulate the background it was subtracted from the measured $^{137}$Cs/$^{60}$Co spectrum. The ratio of the regions free of peaks at the end of the spectra was used as a normalization factor prior to background subtraction, Fig. 5. The net peak areas in the simulated and measured spectra are summarized in Table 5. The $^{137}$Cs and $^{60}$Co sources were placed directly below detector 2 (the middle one) therefore the net counts of detectors 1 and 3 are lower than that of detector 2. The spectra were measured and simulated individually for each detector used in the system. The sums of the three spectra and simulation of the combined system is given in Fig. 6. The net peak areas of the simulated and measured $^{137}$Cs/$^{60}$Co pulse height distributions agreed within 8%, 20%, 6%, and 13%, for the three detectors and their sum, respectively.

## 4. Conclusions

The benchmarks we presented demonstrate the model's ability to represent the system. The model calculations for the Cu foil experiments agreed with the neutron transport flux calculations in soil at four different points within 6–9%. The imprecise locations of the Cu foils contributed to the error in modeling the geometry by MCNP5. The larger discrepancies between the fluxes in positions “c” and “d” are due to lower activations of the foils at these positions. The calculated slope of the calibration line agreed, within 1%, with that derived experimentally.

For Cs and Co PHDs, the increased error in the second (middle) detector may be attributable to a possible error in positioning of the source because of its proximity to the detector. The error in the sum of the spectra was affected by the error in the second detector. The model systematically underestimates the spectra at the low, $<200$ keV, energy region of the Compton continuum. We suspect that the discrepancy arises from additional photon scatterings in the experimental data due to extra scatterings in materials not included in the model. Another source of error is the uncertainty of the Monte Carlo simulations of low-energy electrons [18].

The height optimization experiments demonstrate that the model, in a relative sense, produces similar maximum net peak areas as the experimental ones. The *O* experimental and MCNP5 curves of yield versus height had a similar shape and magnitude. The same was true, to a slightly lesser extent for *C*. However, there was substantial disagreement between MCNP5 and experimental curves for Si. Overall, the presented benchmarking achieved the desired agreement within 10% of the measured parameters except for the area in the central detector when simulating the pulse height distributions.

## References

[1] K.A. Sudduth, J.W. Hummel, Trans. ASAE 39 (1996) 1599.
[2] C.D. Christy, P. Drummond, D.A. Laird, ASAE Paper No. 031044.
[3] M.H. Ebinger, M.L. Norfleet, D.D. Breshears, D.A. Cremers, M.J. Ferris, P.J. Unkefer, M.S. Lamb, K.L. Goddard, C.W. Meyer, Soil Sci. Soc. Am. J. 67 (2003) 1616.
[4] L. Wielopolski, A. Chatterjee, S. Mitra, R. Lal, Geoderma 160 (2011) 394.
[5] J.F. Breismeister, MCNP – A General Purpose Monte Carlo N-Particle Transport Code, Version 4A, Los Alamos National Laboratory, NM, LA–12625–M, 1993.
[6] S.M. Girard, J.B. Shinn, MCNP – A General Monte Carlo N-Particle Transport Code, Version 5, Report LA–CP–03–0245, , 2003.
[7] J. Csikai, Nuclear Data for Geology and Mining, in: S.M. Qaim (Ed.), Nuclear Data for Science and Technology, Spring-Verlag, 1991, pp. 644–649.
[8] C.G. Clayton, C.F. Coleman, Int. J. Appl. Radiat. Isot. 36 (1985) 757.
[9] L. Wielopolski, Z. Song, I. Orion, A.L. Hanson, G. Hendry, Appl. Radiat. Isot. 62 (2005) 97.
[10] L. Wielopolski, H. George, K. Johnsen, S. Mitra, S.A. Prior, H.H. Rogers, H.A. Torbert, Soil Sci. Soc. Am. J. 72 (2008) 1269.

[11] J.M. Puzovic, I.V. Anicin, Nucl. Instrum. Methods A 414 (1998) 279.
[12] W.R. Nelson, H. Hirayama, D. Rogers, The EGS4 Code, SLAC 265 (1985).
[13] S.L. Howell, R.A. Sigg, F.S. Moore, T.A. Devol, J. Radiat. Nucl. Chem. 244 (2000) 173.
[14] H. Choi, G. Roh, Nucl. Sci. Eng. 146 (2004) 188.
[15] MF Physics Corporation, Technical Bulletin, 109.
[16] R.L. Heath, The Texas Convention on the measurement of 14-MeV neutron fluxes, from accelerators, in: Proceeding of the 1965 International Conference on Modern Trends in Activation Analysis, College Station, Texas, 1965.
[17] G.E. Knoll, Radiation Detection and Measurement, third ed., John Wiley and Sons, Inc., Hoboken, NJ, 2000.
[18] S. Hu-Xia, C. Bo-Xian, L. Ti-Zhu, Y. Di, Appl. Radiat. Isot. 57 (2002) 517.